

Production of atomic hydrogen by cosmic rays in dark clouds

Marco Padovani¹, Daniele Galli¹, Alexei V. Ivlev², Paola Caselli², Andrea Ferrara³

¹ INAF–Osservatorio Astrofisico di Arcetri, Largo E. Fermi 5, 50125 Firenze, Italy
e-mail: [padovani, galli]@arcetri.astro.it

² Max-Planck-Institut für Extraterrestrische Physik, Giessenbachstr. 1, 85741 Garching, Germany
e-mail: [ivlev, caselli]@mpe.mpg.de

³ Scuola Normale Superiore, Piazza dei Cavalieri 7, 56126 Pisa, Italy
e-mail: andrea.ferrara@sns.it

September 13, 2018

ABSTRACT

Context. The presence of small amounts of atomic hydrogen, detected as absorption dips in the 21 cm line spectrum, is a well-known characteristic of dark clouds. The abundance of hydrogen atoms measured in the densest regions of molecular clouds can be only explained by the dissociation of H₂ due to cosmic rays.

Aims. We want to assess the role of Galactic cosmic rays in the formation of atomic hydrogen, by using recent developments in the characterisation of the low-energy spectra of cosmic rays and advances in the modelling of their propagation in molecular clouds.

Methods. We model the attenuation of the interstellar cosmic rays entering a cloud and compute the dissociation rate of molecular hydrogen due to collisions with cosmic-ray protons and electrons as well as fast hydrogen atoms. We compare our results with the available observations.

Results. The cosmic-ray dissociation rate is entirely determined by secondary electrons produced in primary ionisation collisions. These secondary particles constitute the only source of atomic hydrogen at column densities above $\sim 10^{21}$ cm⁻². We also find that the dissociation rate decreases with column density, while the ratio between the dissociation and ionisation rates varies between about 0.6 and 0.7. From comparison with observations we conclude that a relatively flat spectrum of interstellar cosmic-ray protons, as the one suggested by the most recent Voyager 1 data, can only provide a lower bound for the observed atomic hydrogen fraction. An enhanced spectrum of low-energy protons is needed to explain most of the observations.

Conclusions. Our findings show that a careful description of molecular hydrogen dissociation by cosmic rays can explain the abundance of atomic hydrogen in dark clouds. An accurate characterisation of this process at high densities is crucial for understanding the chemical evolution of star-forming regions.

Key words. ISM: cosmic rays – ISM: clouds – atomic processes – molecular processes

1. Introduction

The formation of molecular hydrogen occurs on dust grains in molecular clouds through the reaction between two hydrogen atoms. Being an exothermic process, H₂ is then released into the gas phase. Depending on position in the cloud (or the amount of visual extinction measured inward from the cloud’s edge), two processes determine the destruction of H₂ and the restoration of the atomic form: photodissociation due to interstellar (hereafter IS) UV photons and dissociation due to cosmic rays (hereafter CRs). In the diffuse part of molecular clouds, UV photons regulate the abundance of atomic hydrogen by dissociating H₂, while in the densest parts IS UV photons are blocked by dust absorption as well as by H₂ line absorption (Hollenbach et al. 1971). In the deepest parts of the cloud, CRs dominate the destruction of molecular hydrogen.

A wealth of studies have been carried out to characterise the origin of the atomic hydrogen component in dense environments (e.g. McCutcheon et al. 1978; van der Werf et al. 1988; Montgomery et al. 1995; Li & Goldsmith 2003; Goldsmith & Li 2005), but the rate of CR dissociation was always assumed to be constant (i.e., independent of the position in the cloud) or simply neglected. In this paper we want to explore in more detail the role of CRs – especially after the latest data release of the Voyager 1 spacecraft (Cummings et al. 2016), showing that

the measured proton and electron fluxes are not able to explain the values of the CR ionisation rate estimated in diffuse clouds (e.g. Indriolo et al. 2015; Phan et al. 2018). In our previous work (e.g. Padovani et al. 2009; Padovani & Galli 2013; Padovani et al. 2013; Ivlev et al. 2015; Padovani et al. 2018) we postulated the presence of a low-energy component in the IS CR proton spectrum, with which it is possible to recover the high ionisation rates observed in diffuse clouds.

We treat a cloud as a semi-infinite slab. Such a simplification is completely justified for our purposes, for the following reasons. First, attenuation of IS UV photons occurs in a thin gas layer near the cloud’s surface (with a visual extinction of $A_V \approx 1 - 3$ mag), i.e., at column densities much smaller than those characterising the line-of-sight thickness of a cloud. Second, CRs propagate through a cloud along the local magnetic field. The latter assumption is always valid since the Larmor radius of sub-relativistic CRs is much smaller than any characteristic spatial scale of the cloud (Padovani & Galli 2011) and the correlation length of the magnetic field (Houde et al. 2009). Therefore, irrespective of the field geometry, we can measure the coordinate along the local field line and treat the problem as one-dimensional (Padovani et al. 2018)¹. One can straightforwardly

¹ The CR ionisation rate is then a function of the *effective* column density, measured along the field line. To facilitate the presentation of our

generalise these considerations to a slab of a finite thickness by adding IS particles entering the cloud from the opposite side; however, given a strong attenuation, this addition is only important for clouds with column densities of $\approx 10^{22} \text{ cm}^{-2}$ or less (increasing the ionisation and dissociation rates in the cloud's centre by up to a factor of 2).

The paper is organised as follows: in Sect. 2 we discuss the main processes of H_2 dissociation by CR protons, electrons, and fast hydrogen atoms, and carefully compute the resulting dissociation rate as a function of the column density; in Sect. 3 we present equations to compute the fractions of atomic and molecular hydrogen; in Sect. 4 we compare our theoretical findings with available observations; in Sect. 5 we discuss implications for our outcomes and summarise the most important results.

2. CR dissociation reactions with H_2

We consider dissociation processes induced by CR primary and secondary electrons, CR protons, and fast hydrogen atoms colliding with molecular hydrogen. A schematic diagram of different dissociation paths is depicted in Fig. 1.

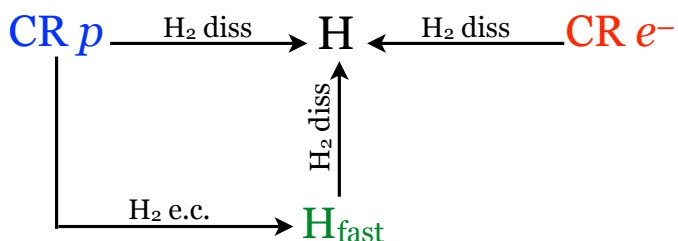


Fig. 1. Dissociation diagram showing the three main processes of production of atomic hydrogen. Labels “diss” and “e.c.” refer to dissociation and electron capture, respectively.

2.1. Electron impact

Electrons can produce atomic hydrogen through excitation of five electronic states of the H_2 triplet ($a^3\Sigma_g^+$, $b^3\Sigma_u^+$, $c^3\Pi_u$, $e^3\Sigma_u^+$, and $d^3\Pi_u$) followed by dissociation. While the radiative decay from the state $b^3\Sigma_u^+$ is fully dissociative, the decay from $e^3\Sigma_u^+$ contributes to dissociation at 20%, and dissociation from the other states is negligible². Thus, the dissociation cross section by electron impact is given by

$$\sigma_{\text{diss}}^e \approx \sigma_{\text{exc}}^e(X \rightarrow b^3\Sigma_u^+) + 0.2\sigma_{\text{exc}}^e(X \rightarrow e^3\Sigma_u^+). \quad (1)$$

2.2. Proton impact

Atomic hydrogen can also be produced by protons, by direct dissociation of H_2 from the vibrational state $v = 0$. The H_2 excitation cross sections by electrons, σ_{exc}^e , and the dissociation cross section by protons, σ_{diss}^p , have been parameterised by Janev et al. (2003) as

$$\sigma(E) = \frac{a}{E^{\alpha_1}} \left[1 - \left(\frac{E_0}{E} \right)^{\alpha_2} \right]^{\alpha_3} \times 10^{-16} \text{ cm}^2, \quad (2)$$

results, in this paper we assume the line-of-sight and the effective column densities to be the same.

² There is also a contribution from the H_2 singlet state, but the respective cross section peaks at about 40 – 50 eV with a maximum value of $3.02 \times 10^{-18} \text{ cm}^2$, which is a factor ≈ 20 lower than the peak value of the triplet-state cross section.

with the energy E in eV. In Table 1 we list the values of factor a , exponents $\alpha_{1,2,3}$, and the energy threshold E_0 for the respective cross sections.

2.3. Fast hydrogen atom impact

Figure 2 shows that dissociation cross sections peak at very low energy, about 8 and 15 eV for protons and electrons, respectively, so one has to carefully look into the processes that regulate the distributions of different species in this energy range. In Appendix A we demonstrate that CR protons are efficiently neutralised at low energies because of electron capture (see also Chabot 2016). This generates a flux of fast H atoms (hereafter H_{fast}) that, in turn, creates fast H^+ ions (“secondary” CR protons) through the reaction (A.3). We compute the equilibrium distributions of protons and H_{fast} atoms, finding that below $\approx 10^4$ eV less than 10% of (non-molecular) hydrogen is in the form of H^+ (see Fig. A.2 in Appendix A), so that the dissociation by H_{fast} (reaction A.4) must be taken into account. The corresponding cross section, $\sigma_{\text{diss}}^{\text{H}}$ (Dove & Mandy 1986; Esposito & Capitelli 2009) is also plotted in Fig. 2.

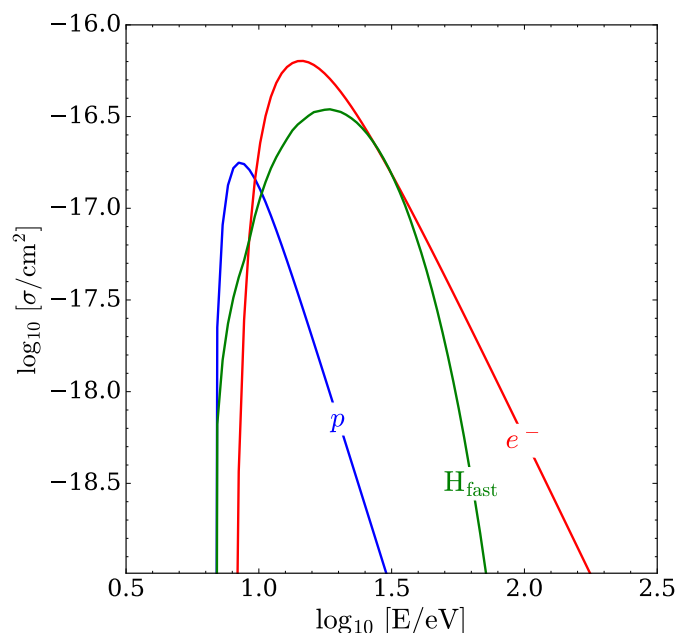


Fig. 2. The energy dependence of the dissociation cross sections by protons (blue), electrons (red), and fast hydrogen atoms (green) colliding with molecular hydrogen.

2.4. CR dissociation rate

The rate of dissociation due to primary and secondary CRs and H_{fast} atoms, occurring at the total column density N , is given by

$$\zeta_{\text{diss}}^k(N) = 2\pi\ell \int j_k(E, N) \sigma_{\text{diss}}^k(E) dE, \quad (3)$$

where j_k is the differential flux of CR particles k , σ_{diss}^k is the dissociation cross section, and $k = p, e, \text{H}_{\text{fast}}$. In the semi-infinite slab geometry, the factor ℓ is equal to 1 for primary CRs and H_{fast} , and to 2 for secondary electrons (because the latter are produced isotropically). The final expression for the dissociation

Table 1. Parameters for the proton dissociation cross section and the (relevant) electron excitation cross sections (Eq. 2).

Reaction	a	α_1	α_2	α_3	E_0 [eV]
$p + \text{H}_2 \rightarrow p + \text{H} + \text{H}$	7.52×10^3	4.64	5.37	2.18	6.72
$e + \text{H}_2 \rightarrow e + \text{H}_2^*(b^3\Sigma_u^+)$	5.57×10^3	3.00	2.33	3.78	7.93
$e + \text{H}_2 \rightarrow e + \text{H}_2^*(e^3\Sigma_u^+)$	4.17×10^2	3.00	4.50	1.60	13.0

rate is obtained by averaging over the pitch-angle distribution of the incident CRs (see Eq. 45 in Padovani et al. 2018).

In the following we assume the same IS CR proton and electron spectra as in Ivlev et al. (2015) and Padovani et al. (2018). For CR protons we adopt two different models: the first one, model \mathcal{L} , is an extrapolation of the Voyager 1 observations to lower energies; the second one, model \mathcal{H} , is characterised by an enhanced flux of low-energy protons with respect to Voyager 1 data. Models \mathcal{L} and \mathcal{H} can be regarded as the lower and the upper bound, respectively, of the average Galactic CR proton spectrum, since the corresponding CR ionisation rates encompass the values estimated from observations in diffuse clouds (e.g. Indriolo et al. 2015; Neufeld & Wolfire 2017). For CR electrons, we use a single model based on the latest Voyager results, which show that the electron flux varies at $E \lesssim 100$ MeV as $\propto E^{-1.3}$ (Cummings et al. 2016). Figure 3 shows the partial contributions to the dissociation rate of primary CR protons and electrons, H_{fast} atoms, and secondary electrons. The latter is computed following Eq. (16) in Ivlev et al. (2015). In Fig. 3 we also show the corresponding visual extinction, $A_V = 5.32 \times 10^{-22} (N/\text{cm}^{-2})$. One can see that ζ_{diss} is entirely dominated by low-energy secondary electrons, produced during the propagation of primary CRs.

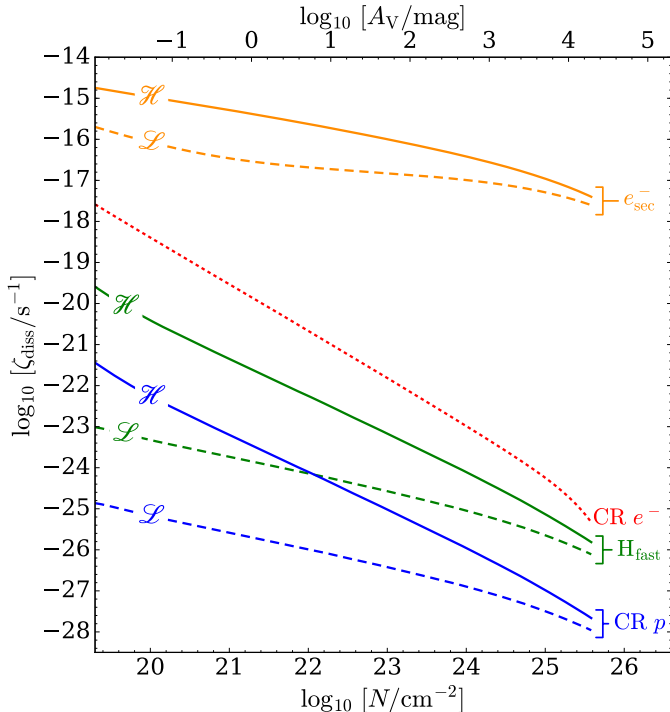


Fig. 3. CR dissociation rate for models \mathcal{L} and \mathcal{H} (dashed and solid lines, respectively) as a function of the total column density of hydrogen (bottom scale) and visual extinction (top scale). The contributions of primary CR protons (blue) and electrons (red dotted), secondary electrons (orange), and fast H atoms (green) are shown.

In previous work (e.g., Li & Goldsmith 2003; Goldsmith & Li 2005), ζ_{diss} has usually been assumed to be equal to the CR ionisation rate, ζ_{ion} (which, in turn, did not depend on N). In Fig. 4 we show that ζ_{diss} and ζ_{ion} exhibit very similar behaviour, decreasing monotonically with N ; the ratio $\zeta_{\text{diss}}/\zeta_{\text{ion}}$ can be as small as ≈ 0.63 at low column densities ($N \approx 10^{19} \text{ cm}^{-2}$), depending on the assumed spectrum of IS CR protons. This ratio rapidly approaches the constant value of ≈ 0.7 , and at $N \gtrsim 10^{22} \text{ cm}^{-2}$ becomes independent of the column density and the IS proton spectrum. The values of ζ_{diss} and ζ_{ion} are comparable because secondary electrons provide the major contribution to both processes. We note that the ionisation rate has been computed by taking into account the presence of H_{fast} atoms (see Eq. B.1 in Appendix B), contributing to the production of H_2^+ ions through the reaction (A.2) at energies below $\approx 10^4$ eV. However this process is only marginally important for model \mathcal{H} below $N \approx 10^{21} \text{ cm}^{-2}$, and is always negligible for model \mathcal{L} (see Appendix B). Figure 4 also shows the photodissociation rate, $\zeta_{\text{pd}} = D_0\chi_a$, computed following Draine (2011).

3. Balance equation

Goldsmith & Li (2005) and Goldsmith et al. (2007) presented a time-dependent modelling of the H abundance in molecular clouds and introduced the concept of atomic-to-molecular hydrogen ratio, $n_{\text{H}}/n_{\text{H}_2}$, as a clock of the cloud's evolutionary stage. In particular, Goldsmith & Li (2005) modelled observations of $n_{\text{H}}/n_{\text{H}_2}$ in five dark clouds, concluding that the characteristic time required to reach a steady-state $n_{\text{H}}/n_{\text{H}_2}$ ratio is close to the cloud ages. In the following, we consider the steady-state solution, keeping in mind that time dependence may still affect the interpretation of the observational data (see Sect. 4.1).

In steady-state, the balance between H_2 formation and destruction processes gives

$$Rnn_{\text{H}} = n_{\text{H}_2} (D_0\chi_a + \zeta_{\text{diss}}). \quad (4)$$

Here, $n = n_{\text{H}} + 2n_{\text{H}_2}$ is the total volume density of hydrogen, R is the H_2 formation rate coefficient, D_0 is the unattenuated photodissociation rate, χ_a is the attenuation factor for dust absorption and H_2 -self shielding, and ζ_{diss} is the CR dissociation rate. In the following we assume $R = 3 \times 10^{-17} \text{ cm}^3 \text{ s}^{-1}$ (Jura 1975) and $D_0 = 2 \times 10^{-11} G_0 \text{ s}^{-1}$ (Draine 2011, taking into account a semi-infinite slab geometry), where G_0 is the FUV radiation field in Habing units (Habing 1968). Unless specified otherwise, we adopt $G_0 = 1$. The attenuation factor is usually written in the form

$$\chi_a(N, N_{\text{H}_2}) = \chi_{\text{sh}}(N_{\text{H}_2})e^{-\tau(N)}, \quad (5)$$

where $\chi_{\text{sh}}(N_{\text{H}_2}) = (10^{14} \text{ cm}^{-2}/N_{\text{H}_2})^{0.75}$ is the H_2 self-shielding factor (Tielens 2010, valid for $10^{14} \text{ cm}^{-2} \lesssim N_{\text{H}_2} \lesssim 10^{21} \text{ cm}^{-2}$) and $\tau(N) = \sigma_{\text{g}}N$ is the dust attenuation. Here, $N = N_{\text{H}} + 2N_{\text{H}_2}$ is the total column density of hydrogen and $\sigma_{\text{g}} = 1.9 \times 10^{-21} \text{ cm}^2$ is the average value of the FUV dust grain absorption cross section for solar metallicity (Draine 2011).

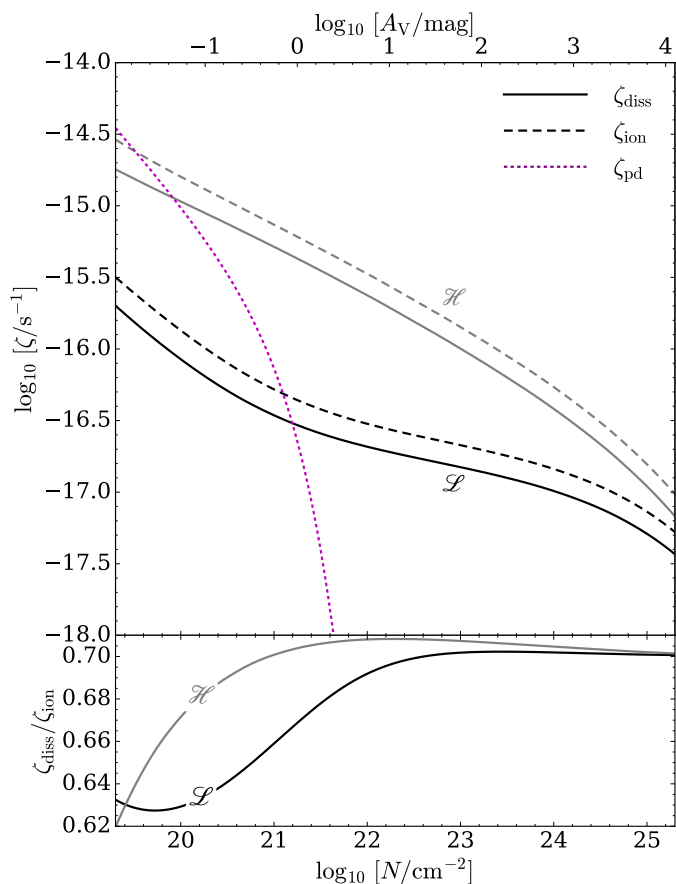


Fig. 4. Upper panel: rates of CR dissociation (ζ_{diss} , solid lines), CR ionisation (ζ_{ion} , dashed lines), and photodissociation (ζ_{pd} , purple dotted line) for models \mathcal{L} (black) and \mathcal{H} (grey), plotted versus the total column density of hydrogen (bottom scale) and visual extinction (top scale). Lower panel: ratio $\zeta_{\text{diss}}/\zeta_{\text{ion}}$ for the two models.

Assuming $n_{\text{H}}/n = dN_{\text{H}}/dN$ and $n_{\text{H}_2}/n = dN_{\text{H}_2}/dN$, Eq. (4) becomes

$$\frac{dN_{\text{H}_2}}{dN} = \left(2 + \frac{D_0 \chi_a + \zeta_{\text{diss}}}{Rn} \right)^{-1}. \quad (6)$$

The fractions of atomic and molecular hydrogen can be expressed as

$$f_{\text{H}} = \frac{n_{\text{H}}}{n_{\text{H}} + n_{\text{H}_2}} = \frac{1 - 2dN_{\text{H}_2}/dN}{1 - dN_{\text{H}_2}/dN} \quad (7)$$

and

$$f_{\text{H}_2} = 1 - f_{\text{H}} = \frac{dN_{\text{H}_2}/dN}{1 - dN_{\text{H}_2}/dN}, \quad (8)$$

respectively. In the next section we describe in detail all the processes that contribute to the dissociation of molecular hydrogen.

4. Comparison with observations

Li & Goldsmith (2003) performed a survey of dark clouds in the Taurus-Perseus region, and reported the detection of H I narrow self-absorption features. This allowed them to compute the atomic and molecular hydrogen fraction (Eqs. 7 and 8). They concluded that a relevant fraction of atomic hydrogen is mixed

with H₂ in the densest part of a cloud, shielded from the IS UV flux.

At high column densities typical of dark clouds, the attenuation factor χ_a in Eq. (4) is so large that the UV photodissociation is inefficient, and the observed $n_{\text{H}}/n_{\text{H}_2}$ ratios can only be explained by CR dissociation. In Sect. 2.4, we showed that $\zeta_{\text{diss}} \approx 0.7\zeta_{\text{ion}}$ at typical column densities of dark clouds ($\approx 10^{22} \text{ cm}^{-2}$); more importantly, ζ_{diss} is not constant, but decreases with N (e.g., Padovani et al. 2009, 2018).

We compute the fraction of atomic and molecular hydrogen expected at different column densities (Eqs. 7 and 8), to evaluate the effect of CR dissociation on the abundance of atomic hydrogen in dark clouds. For the total volume density n in Eq. (4), we use the average value of $5 \times 10^3 \text{ cm}^{-3}$ computed by Li & Goldsmith (2003), to which we add an error of $2.6 \times 10^3 \text{ cm}^{-3}$ (the standard deviation for the observed values).

Figure 5 shows the comparison between our models and the observations by Li & Goldsmith (2003). As expected, UV photodissociation alone cannot explain the observed $n_{\text{H}}/n_{\text{H}_2}$ ratios because of the attenuation at large column densities. More notably, a CR spectrum based on the extrapolation of the Voyager data (model \mathcal{L}) fails to reproduce the majority of the observations, and only a spectrum enhanced at low energies (such as model \mathcal{H}) can explain this. The latter fact corroborates the need of a low-energy tail in the IS CR flux of protons, also required to explain the high CR ionisation rates in diffuse clouds (e.g. Padovani et al. 2009; Indriolo et al. 2015).

4.1. Uncertainties of the H₂ formation rate

The large spread in the observed values of f_{H} probably reflects a broad variety of environments in dark clouds, including, e.g., variations in the density and IS UV radiation field (see e.g. Bialy & Sternberg 2016). In this work we assume a H₂ formation rate of $R = 3 \times 10^{-17} \text{ cm}^3 \text{ s}^{-1}$ (see Sect. 3)³. However, R is strongly dependent on the condition of each cloud; for example, in photodissociation regions, where the large abundance of polycyclic aromatic hydrocarbons favours the formation of H₂, R can increase by one order of magnitude (Habart et al. 2004). Variations in the grain size distribution may also change the value of R by a factor of ~ 3 (Goldsmith & Li 2005). Draine (2011) suggests $R \approx 3 \times 10^{-17} \sqrt{T/70 \text{ K}} \text{ cm}^3 \text{ s}^{-1}$, but even assuming T as low as 10 K, we find $f_{\text{H}} \approx 10^{-3}$ at $N \approx 10^{22} \text{ cm}^{-2}$ for a Voyager-like spectrum (model \mathcal{L}). As a consequence, a larger flux of low-energy CR protons (model \mathcal{H}) is still needed to explain the higher $n_{\text{H}}/n_{\text{H}_2}$ ratios. This conclusion remains unchanged even if G_0 is increased by up to two orders of magnitude, since the UV field is exponentially attenuated in the range of column densities of the observed dark clouds ($2 \times 10^{21} \text{ cm}^{-2} \lesssim N \lesssim 2 \times 10^{22} \text{ cm}^{-2}$).

One should also keep in mind that, as mentioned in Sect. 3, some of the observed clouds may have not necessarily reached a steady-state $n_{\text{H}}/n_{\text{H}_2}$ ratio (Goldsmith & Li 2005; Goldsmith et al. 2007). In this case, model \mathcal{L} could not be completely ruled out as, if these clouds are younger, they will have higher $n_{\text{H}}/n_{\text{H}_2}$ ratio than predicted by our steady-state assumption.

³ We note that Li & Goldsmith (2003) used $R = 6.5 \times 10^{-18} \text{ cm}^3 \text{ s}^{-1}$, which is a factor of ≈ 5 smaller than our value. A lower R implies a lower ionisation rate needed to reproduce the observations. This explains why, using a constant dissociation rate equal to the ionisation rate of $3 \times 10^{-17} \text{ s}^{-1}$, they found $f_{\text{H}} \approx 1.5 \times 10^{-3}$.

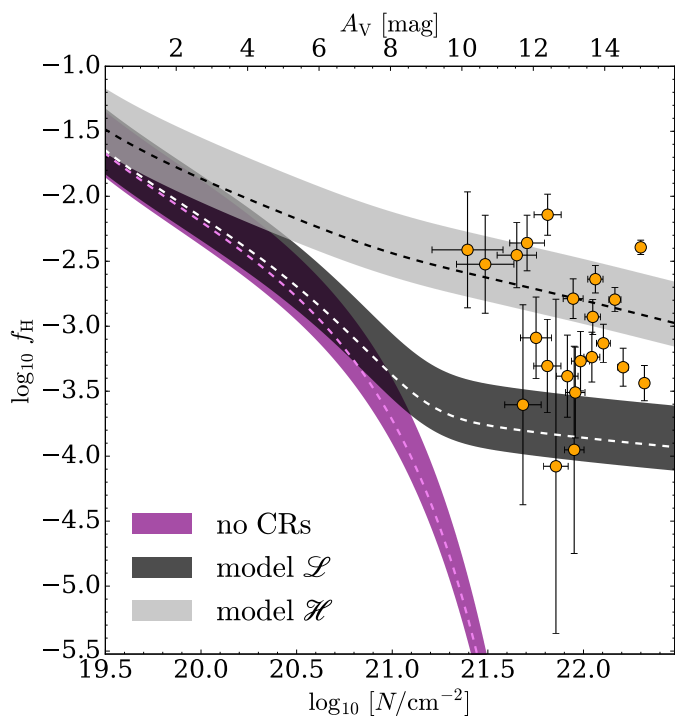


Fig. 5. Atomic hydrogen fraction versus the total column density of hydrogen (bottom scale) and visual extinction (top scale). Observations from Li & Goldsmith (2003) are shown as *solid orange circles*. *Coloured stripes* represent our results for the case of photodissociation only (*purple*), model \mathcal{L} (*black*), and \mathcal{H} (*grey*). *Dashed lines* refer to the average value of the total volume density of hydrogen (suggested by Li & Goldsmith 2003).

5. Discussion and conclusions

Dissociation of H_2 into atomic hydrogen by CRs in dark clouds can have important consequences for the chemical evolution of dense regions in the clouds. Atomic hydrogen is the most mobile reactive species on the surface of bare dust grains and icy mantles, and therefore it is crucial to accurately determine its abundance. The larger f_{H} values predicted in this work imply a more efficient hydrogenation of molecular species on grain surfaces. In particular, hydrogenation of CO, which freezes out onto grains at densities above a few 10^4 cm^{-3} (e.g., Caselli et al. 1999), follows the sequence (e.g. Tielens & Hagen 1982)



This leads to efficient production of formaldehyde (H_2CO) and methanol (CH_3OH ; Vasyunin et al. 2017) on very short time scales. Hence, even if dissociation by energetic particles takes place, CO cannot be returned to the gas phase, because it is rapidly converted into methanol. If the products of dissociation do not move very far from their formation site (Shingledecker et al. 2018), methanol is ejected from the surface. This is because the exothermicity of chemical reactions (9) is partially channeled into kinetic energy through a process known as reactive desorption (Garrod et al. 2007). On the other hand, ammonia (NH_3), which is synthesised onto grains through the hydrogenation sequence (e.g. Hiraoka et al. 1995; Fedoseev et al. 2015)



can, in principle, go back to the gas phase upon surface dissociation followed by reactive desorption. These considerations could

help in explaining the observational evidence that NH_3 (unlike CO) does not appear to deplete towards the central regions of dense cores, despite its large binding energy. To verify this hypothesis, one should carefully evaluate the consequences of an enhanced abundance of atomic hydrogen in chemical models.

We point out that CR dissociation is not only limited to H_2 , but could occur for other molecular species as well, both in the gas phase and on/in ices mantles, with potentially significant consequences in the chemical composition of dense cloud cores and dark clouds.

To summarise, in this paper we studied the role of CRs in determining the fractional abundance of atomic hydrogen in dark clouds. The main results are:

- (i) The CR dissociation rate, ζ_{diss} , is primarily determined by secondary electrons produced during the primary CR ionisation process. These secondary electrons can efficiently dissociate H_2 and represent the only source of atomic hydrogen at column densities larger than $\approx 10^{21} \text{ cm}^{-2}$, regulating the $n_{\text{H}}/n_{\text{H}_2}$ ratio in dark clouds;
- (ii) ζ_{diss} entering the balance equation (4) is not equal to the ionisation rate ζ_{ion} , as assumed in some previous work. We find that the ratio $\zeta_{\text{diss}}/\zeta_{\text{ion}}$ varies between ≈ 0.63 and ≈ 0.7 , depending on the column density range, while ζ_{ion} is a decreasing function of the column density;
- (iii) Even given the uncertainties in the values of H_2 formation rate, temperature, total hydrogen volume density, and IS UV radiation field for each cloud, only a CR proton spectrum enhanced at low energies (such as our model \mathcal{H}) is capable to reproduce the upper values of measured f_{H} , under the assumption of steady state. We note that neither model \mathcal{L} nor \mathcal{H} is able to reproduce the entire set of observational data: the spread in the values of f_{H} at any given column density must be attributed to time dependence or to individual characteristics of each cloud. For example, tangled magnetic field lines and/or higher volume densities would result in a stronger CR attenuation and therefore in a lower f_{H} ;
- (iv) An accurate description of H_2 dissociation in dense environments is essential, because many chemical processes (such as CO hydrogenation and its depletion degree onto dust grains, or formation of complex organic molecules) critically depend on the abundance of atomic hydrogen.

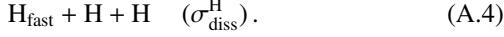
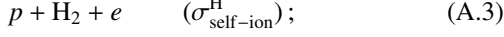
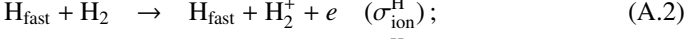
Acknowledgements. The authors wish to thank the referee, Paul Goldsmith, for his careful reading of the manuscript and insightful comments that considerably helped to improve the paper. MP acknowledges funding from the European Union's Horizon 2020 research and innovation programme under the Marie Skłodowska-Curie grant agreement No 664931. AF acknowledges support from the ERC Advanced Grant INTERSTELLAR H2020/740120. The authors thank Fabrizio Esposito for sending us his results for the H_2 dissociation cross section by atomic hydrogen impact.

Appendix A: Equilibrium distribution of protons and H_{fast} atoms at low energies

Because of the process of electron capture at low energies, CR protons interacting with H_2 are efficiently neutralised,



creating fast H atoms⁴. At the same time, H_{fast} atoms reacting with H_2 yield



The electron capture by protons, Eq. (A.1), and the reaction of H_{fast} self-ionisation, Eq. (A.3), are catastrophic processes, since the respective projectile particles disappear after such collisions. The reactions of H_2 ionisation and dissociation by H_{fast} atoms, Eqs. (A.2) and (A.4), respectively, are continuous loss processes, where the projectile kinetic energy decreases only slightly after each collision. The efficiency of continuous energy losses is generally characterised by the projectile's stopping range (see, e.g. Padovani et al. 2009).

For our calculations, $\sigma_{\text{e.c.}}^p$ is taken from Rudd et al. (1983), σ_{ion}^H is from Phelps (1990) and Kunc & Soon (1991), $\sigma_{\text{self-ion}}^H$ is computed by Stier & Barnett (1956), van Zyl et al. (1981), and Phelps (1990), and σ_{diss}^H is from Dove & Mandy (1986) and Esposito & Capitelli (2009). In Fig. A.1 we plot the cross sections and the inverse of the proton stopping range, R_p^{-1} , versus the respective projectile's energy. We see that $\sigma_{\text{e.c.}}^p$ is much larger than R_p^{-1} for $10^2 \text{ eV} \lesssim E \lesssim 10^5 \text{ eV}$, which implies that continuous loss processes cannot significantly affect the balance between protons and H_{fast} atoms at these energies. The equilibrium ratio of the H_{fast} and proton fluxes is then given by

$$\frac{j_{H_{\text{fast}}}}{j_p} \approx \frac{\sigma_{\text{e.c.}}^p}{\sigma_{\text{self-ion}}^H}. \quad (\text{A.5})$$

This allows us to calculate the fractions of H_{fast} atoms,

$$f_{H_{\text{fast}}} = \frac{j_{H_{\text{fast}}}}{j_{H_{\text{fast}}} + j_p} = \frac{\sigma_{\text{e.c.}}^p}{\sigma_{\text{e.c.}}^p + \sigma_{\text{self-ion}}^H}, \quad (\text{A.6})$$

and protons, $f_p = 1 - f_{H_{\text{fast}}}$. Figure A.2 shows that for energies below $\approx 10^4 \text{ eV}$, only less than 10% of non-molecular hydrogen is in the form of protons. This means that H_2 ionisation at these energies is dominated by H_{fast} atoms, via reaction (A.2).

Appendix B: Ionisation by H_{fast} atoms

As shown in Appendix A, the ionisation at energies below $\approx 10^4 \text{ eV}$ is mostly driven by H_{fast} atoms. To take this effect into account, we use the following expression for the H_2 ionisation rate by CR protons:

$$\zeta_{\text{ion}}^p(N) = 2\pi \int \left\{ j_p(E, N) \left[\sigma_{\text{ion}}^p(E) + \sigma_{\text{e.c.}}^p(E) \right] + j_{H_{\text{fast}}}(E, N) \sigma_{\text{ion}}^H(E) \right\} dE, \quad (\text{B.1})$$

where σ_{ion}^p is the H_2 ionisation cross section by proton impact (Rudd et al. 1985). It turns out, however, that the difference

⁴ In parentheses, we put the cross section of the respective process.

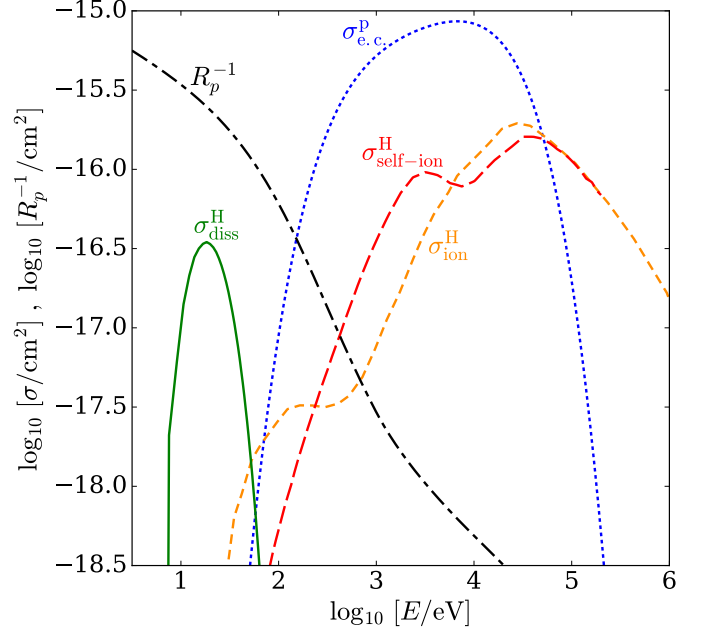


Fig. A.1. The cross sections of processes governing equilibrium distributions of protons and fast hydrogen atoms at low energies: electron capture by p (A.1, dotted blue line), ionisation of H_2 by H_{fast} (A.2, short-dashed orange line), self-ionisation of H_{fast} (A.3, long-dashed red line), and H_2 dissociation by H_{fast} (A.4, solid green line). The inverse of the proton stopping range, R_p^{-1} , is also plotted (black dot-dashed line).

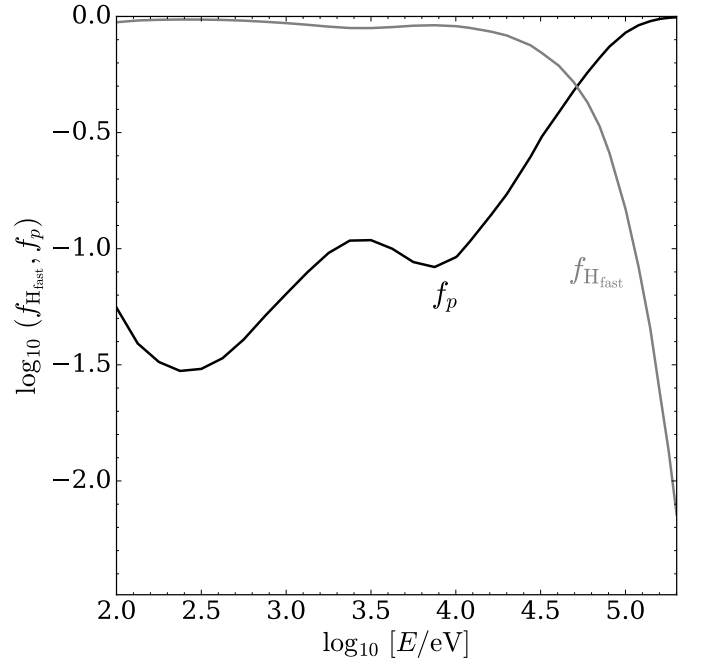


Fig. A.2. Fraction of non-molecular hydrogen in neutral ($f_{H_{\text{fast}}}$) and ionised (f_p) form as a function of the energy.

between the ionisation rates computed from Eq. (B.1) taking into account Eq. (A.5) and assuming $j_{H_{\text{fast}}} = 0$ is very small: for $N \approx 10^{19} \text{ cm}^{-2}$, the difference is $\approx 5\%$ and $\approx 40\%$ for models \mathcal{L} and \mathcal{H} , respectively, at higher column densities it rapidly decreases and becomes negligible for both models above

$\approx 10^{21} \text{ cm}^{-2}$. This result justifies the assumption $j_{\text{H}^{\text{fast}}} = 0$ made previously for calculating the ionisation.

References

- Bialy, S. & Sternberg, A. 2016, *ApJ*, 822, 83
- Caselli, P., Walmsley, C. M., Tafalla, M., Dore, L., & Myers, P. C. 1999, *ApJ*, 523, L165
- Chabot, M. 2016, *A&A*, 585, A15
- Cummings, A. C., Stone, E. C., Heikkilä, B. C., et al. 2016, *ApJ*, 831, 18
- Dove, J. E. & Mandy, M. E. 1986, *ApJ*, 311, L93
- Draine, B. T. 2011, *Physics of the Interstellar and Intergalactic Medium*
- Esposito, F. & Capitelli, M. 2009, *Journal of Physical Chemistry A*, 113, 15307
- Fedoseev, G., Ioppolo, S., Zhao, D., Lamberts, T., & Linnartz, H. 2015, *MNRAS*, 446, 439
- Garrod, R. T., Wakelam, V., & Herbst, E. 2007, *A&A*, 467, 1103
- Goldsmith, P. F. & Li, D. 2005, *ApJ*, 622, 938
- Goldsmith, P. F., Li, D., & Krčo, M. 2007, *ApJ*, 654, 273
- Habart, E., Boulanger, F., Verstraete, L., Walmsley, C. M., & Pineau des Forêts, G. 2004, *A&A*, 414, 531
- Habing, H. J. 1968, *Bull. Astron. Inst. Netherlands*, 20, 120
- Hiraoka, K., Yamashita, A., Yachi, Y., et al. 1995, *ApJ*, 443, 363
- Hollenbach, D. J., Werner, M. W., & Salpeter, E. E. 1971, *ApJ*, 163, 165
- Houde, M., Vaillancourt, J. E., Hildebrand, R. H., Chitsazzadeh, S., & Kirby, L. 2009, *ApJ*, 706, 1504
- Indriolo, N., Neufeld, D. A., Gerin, M., et al. 2015, *ApJ*, 800, 40
- Ivlev, A. V., Padovani, M., Galli, D., & Caselli, P. 2015, *ApJ*, 812, 135
- Janev, R. K., Reiter, D., & Samm, U. 2003, *Collision processes in low-temperature hydrogen plasmas*, 188
- Jura, M. 1975, *ApJ*, 197, 575
- Kunc, J. A. & Soon, W. H. 1991, *J. Chem. Phys.*, 95, 5738
- Li, D. & Goldsmith, P. F. 2003, *ApJ*, 585, 823
- McCutcheon, W. H., Shuter, W. L. H., & Booth, R. S. 1978, *MNRAS*, 185, 755
- Montgomery, A. S., Bates, B., & Davies, R. D. 1995, *MNRAS*, 273, 449
- Neufeld, D. A. & Wolfire, M. G. 2017, *ApJ*, 845, 163
- Padovani, M. & Galli, D. 2011, *A&A*, 530, A109
- Padovani, M. & Galli, D. 2013, in *Astrophysics and Space Science Proceedings*, Vol. 34, *Cosmic Rays in Star-Forming Environments*, ed. D. F. Torres & O. Reimer, 61
- Padovani, M., Galli, D., & Glassgold, A. E. 2009, *A&A*, 501, 619
- Padovani, M., Hennebelle, P., & Galli, D. 2013, *A&A*, 560, A114
- Padovani, M., Ivlev, A. V., Galli, D., & Caselli, P. 2018, *ArXiv e-prints* [[arXiv:1803.09348](https://arxiv.org/abs/1803.09348)]
- Phan, V. H. M., Morlino, G., & Gabici, S. 2018, *ArXiv e-prints* [[arXiv:1804.10106](https://arxiv.org/abs/1804.10106)]
- Phelps, A. V. 1990, *Journal of Physical and Chemical Reference Data*, 19, 653
- Rudd, M. E., Goffe, T. V., Dubois, R. D., Toburen, L. H., & Ratcliffe, C. A. 1983, *Phys. Rev. A*, 28, 3244
- Rudd, M. E., Kim, Y.-K., Madison, D. H., & Gallagher, J. W. 1985, *Reviews of Modern Physics*, 57, 965
- Shingledecker, C. N., Tennis, J., Le Gal, R., & Herbst, E. 2018, *ApJ*, 861, 20
- Stier, P. M. & Barnett, C. F. 1956, *Physical Review*, 103, 896
- Tielens, A. G. G. M. 2010, *The Physics and Chemistry of the Interstellar Medium*
- Tielens, A. G. G. M. & Hagen, W. 1982, *A&A*, 114, 245
- van der Werf, P. P., Goss, W. M., & Vanden Bout, P. A. 1988, *A&A*, 201, 311
- van Zyl, B., Le, T. Q., & Amme, R. C. 1981, *J. Chem. Phys.*, 74, 314
- Vasyunin, A. I., Caselli, P., Dulieu, F., & Jiménez-Serra, I. 2017, *ApJ*, 842, 33